The effects of increasing lithium deposition on the power exhaust channel in NSTX



2014 Nucl. Fusion 54 023001

(http://iopscience.iop.org/0029-5515/54/2/023001)

IOP Publishing | International Atomic Energy Agency Nuclear Fusion
Nucl. Fusion **54** (2014) 023001 (7pp) doi:10.1088/0029-5515/54/2/023001

# The effects of increasing lithium deposition on the power exhaust channel in NSTX

**T.K. Gray[1], J.M. Canik[1], R. Maingi[1,2], A.G. McLean[3], J-W. Ahn[1], M.A. Jaworkski[2], R. Kaita[2], M. Ono[2] , S.F. Paul[2] and the NSTX Team**

[1] Oak Ridge National Laboratory, Oak Ridge, TN USA
[2] Princeton Plasma Physics Laboratory, Princeton, NJ USA
[3] Lawrence Livermore National Laboratory, Livermore, CA USA

E-mail: tkgray@pppl.gov

Received 31 December 2012, revised 24 September 2013
Accepted for publication 15 November 2013
Published 21 January 2014

## Abstract

Previous measurements on the National Spherical Torus Experiment (NSTX) demonstrated peak, perpendicular heat fluxes, $q_{\mathrm{dep,pk}} \leqslant 15\,\mathrm{MW\,m^{-2}}$ with an inter-edge localized mode integral heat flux width, $\lambda_{q,\mathrm{int}}^{\mathrm{mid}} \sim 3$–$7\,\mathrm{mm}$ during high performance, high power operation (plasma current, $I_\mathrm{p} = 1.2\,\mathrm{MA}$ and injected neutral beam power, $P_\mathrm{NBI} = 6\,\mathrm{MW}$) when magnetically mapped to the outer midplane. Analysis indicates that $\lambda_{q,\mathrm{int}}^{\mathrm{mid}}$ scales approximately as $I_\mathrm{p}^{-1}$. The extrapolation of the divertor heat flux and $\lambda_q$ for NSTX-U are predicted to be upwards of $24\,\mathrm{MW\,m^{-2}}$ and 3 mm, respectively assuming a high magnetic flux expansion, $f_\mathrm{exp} \sim 30$, $P_\mathrm{NBI} = 10\,\mathrm{MW}$, balanced double null operation and boronized wall conditioning. While the divertor heat flux has been shown to be mitigated through increased magnetic flux expansion, impurity gas puffing, and innovative divertor configurations on NSTX, the application of evaporative lithium coatings in NSTX has shown reduced peak heat flux from 5 to $2\,\mathrm{MW\,m^{-2}}$ during similar operation with 150 and 300 mg of pre-discharge lithium evaporation respectively. Measurement of divertor surface temperatures in lithiated NSTX discharges is achieved with a unique dual-band IR thermography system to mitigate the variable surface emissivity introduced by evaporative lithium coatings. This results in a relative increase in divertor radiation as measured by divertor bolometry. While the measured divertor heat flux is reduced with strong lithium evaporation, $\lambda_q$ contracts to 3–6 mm at low $I_\mathrm{p}$ but remains nearly constant as $I_\mathrm{p}$ is increased to 1.2 MA yielding $\lambda_q$'s comparable to no lithium discharges at high $I_\mathrm{p}$.

Keywords: divertor, heat flux, lithium

(Some figures may appear in colour only in the online journal)

## 1. Introduction

Spherical tokamaks (STs) have advantages over traditional aspect ratio tokamaks in that a potential DEMO fusion reactor or Fusion Nuclear Science Facility (FNSF) could be designed to operate at higher $\beta$ and with a more compact size. However, due to their compact nature, the plasma facing components (PFCs) in divertors of STs can be subject to large heat and particle loads. These unmitigated heat fluxes will erode and possibly destroy the PFCs leading to machine downtime and eventual replacement of the divertor PFCs. Current cooling technologies, such as those implemented for ITER [1], limit the incident divertor heat flux to $\leqslant 10\,\mathrm{MW\,m^{-2}}$. However, the upgraded National Spherical Torus Experiment (NSTX-U) planned for initial operation in 2014 [2] is predicted to experience unmitigated heat fluxes up to $25\,\mathrm{MW\,m^{-2}}$ operating assuming a double-null configuration with a large magnetic flux expansion, $f_\mathrm{exp} \sim 30$ [3]. Because of this, there is currently a major research thrust into mitigating the divertor heat flux for the ST as well as ITER. This could include some combination of a detached or radiative divertor, high $f_\mathrm{exp}$ [3–5], and/or a snowflake divertor [6, 7].

Results from NSTX [8], EAST, smaller limiter tokamaks [9, 10] and stellarators [11] have demonstrated the positive benefits of lithium wall conditioning techniques. These include increased energy confinement time [11, 12], reduced H-mode power threshold [13, 14], reduced divertor recycling [15] and the elimination of edge localized modes (ELMs) [16]. NSTX now routinely uses lithium as a wall conditioning technique instead of boronization [17]. The focus of this work will study the effect of varying amounts of pre-discharge lithium evaporation on the power exhaust channel in NSTX. A discussion of the NSTX experiment and diagnostics used follows in the next section. Section 3 will present results of varying lithium evaporation amounts on the peak divertor heat flux as well as the power scrape-off layer (SOL) width, $\lambda_q$. Finally, section 4 will summarize the observed results.

 

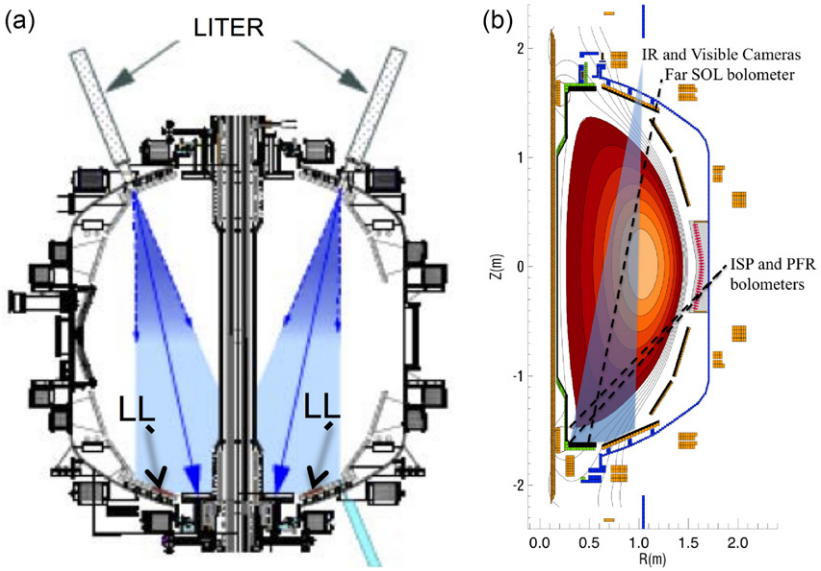


**Figure 1.** (*a*) Schematic of the lithium evaporators (LiTERs) in NSTX used for pre-discharge lithium evaporation to coat the lower divertor surfaces. (*b*) Poloidal cross-section of a typical high $\delta$ NSTX discharge showing diagnostics views of divertor IR and visible cameras as well as divertor bolometers viewing the inner strike point (ISP), private flux region (PFR) and the far scrape-off layer (far SOL).

## 2. Experimental set-up

NSTX is a medium size spherical torus with a major radius, $R_M = 0.85$ m and minor radius, $a_m \leqslant 0.65$ m ($A \geqslant 1.27$). Plasma current, $I_p$ can be varied from 0.6–1.4 MA, with toroidal magnetic field, $B_T$ in the range of 0.35–0.55 T and discharge lengths of $\leqslant$1.8 s. Plasma heating is achieved by neutral beam injection typically ranging in injected power $1 \leqslant P_{NBI} \leqslant 7.4$ MW with core electron temperatures, $T_e(0) = 0.6$–1.5 keV and line-average electron densities, $n_e = (1\text{–}8) \times 10^{19}$ m$^{-3}$.

Since 2006 NSTX has employed evaporative lithium wall conditioning of its ATJ graphite plasma facing surfaces during some or all of the run campaign [17]. Lithium is evaporated onto the lower divertor prior to the discharge from two lithium ovens located on top of NSTX and toroidally displaced by 120° as shown in figure 1(*a*). Typical pre-discharge lithium depositions can range from 10–300 mg though much larger depositions have been used. For boronized discharges, an Indigo Omega IR camera operated at a 30 Hz frame rate is used to measure surface temperature, which is derived from both an *ex situ* calibration with a blackbody calibration source as well as an *in situ* calibration during vacuum bake-outs that takes into account window transmission [18]. For lithiated discharges a fast Santa Barbra Focal Plane IR camera [19], equipped with dual-band optics to capture medium wavelength IR (MWIR: 7–10 $\mu$m) and long wavelength IR (LWIR: 10–13 $\mu$m) images on the camera simultaneously [20], is used to determine the divertor surface temperature independent of changes in surface emissivity due to the lithium evaporation. The dual-band IR camera was operated at 1.6 kHz and used the same calibration procedure as the Indigo Omega IR camera. Heat flux is then determined by a 2D (radial and into the divertor tile) finite difference code THEODOR [21] using the measured divertor surface temperature, $T_{surf}$ as the front face boundary condition. Data from the fast IR camera are then numerically averaged to an equivalent 30 Hz frame rate for comparison with the boronized data set.

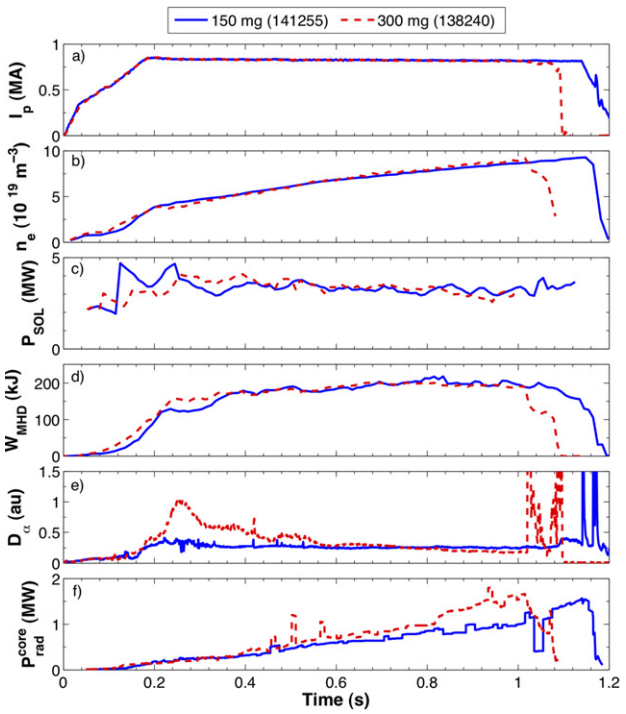


**Figure 2.** Comparison of (*a*) plasma current, $I_p$; (*b*) line-averaged density, $n_e$; (*c*) power crossing the last-closed flux surface, $P_{SOL}$; (*d*) stored energy, $W_{MHD}$; (*e*) divertor $D_\alpha$ emission; and (*f*) core radiated power, $P_{rad}^{core}$ for 150 (——) and 300 mg (- - - -) 0.8 MA discharges and $P_{NBI} = 4$ MW.

Figure 2 shows a comparison between two NSTX discharges with 150 mg and 300 mg of lithium evaporation respectively. Both discharges are otherwise similar with $I_p = 0.8$ MA, $P_{NBI} = 4$ MW, though the 150 mg discharge had some initial pre-heating up to 5 MW from $t = 0.1$–0.25 s,

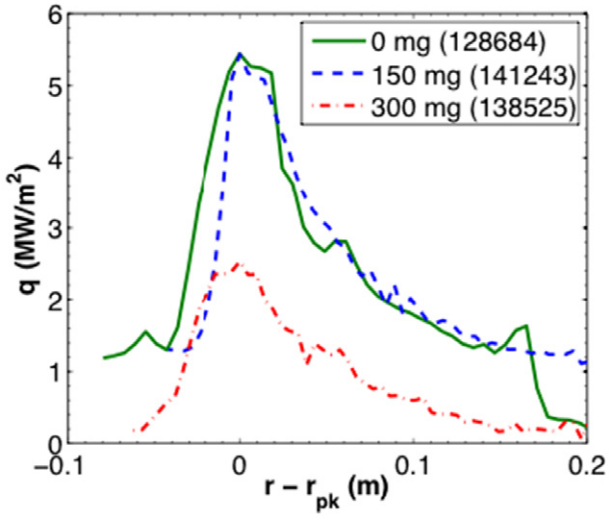


**Figure 3.** Radial heat flux profile for discharges with 0 mg (boronized) (——), 150 mg (- - - -) and 300 mg (— · —) of lithium evaporation before the discharges.

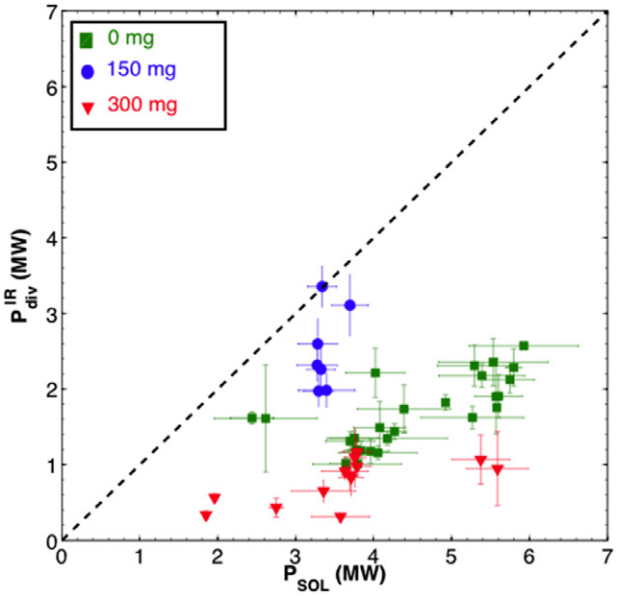


**Figure 4.** Incident divertor power measured at the outer strike point as a function of power crossing the last closed flux surface for 0 (■), 150(●) and 300 mg (▼) of lithium deposition.

and strong plasma shaping with high triangularity, $\delta \sim 0.7$ and elongation, $\kappa \sim 2.2$. The 300 mg discharge also required higher gas puffing to fuel the discharge and avoid locked modes. Figures 2(*c*) and (*d*) show similar line averaged core densities and stored energies. The power crossing through the last-closed flux surface, $P_{\rm SOL}$, which is given by $P_{\rm SOL} = P_{\rm oh} + P_{\rm NBI} - P_{\rm core}^{\rm rad} - {\rm d}W_{\rm p}/{\rm d}t$, where $P_{\rm oh}$ is the ohmic heating power, $P_{\rm rad}^{\rm core}$ is the core radiated power and ${\rm d}W_{\rm p}/{\rm d}t$ is the time rate of change of the plasma energy, is shown in figure 2(*c*). Other than the initial pre-heating differences from 0.1–0.25 s, $P_{\rm SOL}$ is comparable between the two discharges.

## 3. Results

It has been previously reported that the addition of lithium to the divertor of NSTX had the effect of narrowing the heat flux width, $\lambda_q$ [3]. Given that $P_{\rm SOL}$ is similar for the 150 and 300 mg discharges, one would expect the peak heat flux to increase as $\lambda_q$ contracts to conserve power. However, as shown in figure 3, the peak deposited heat flux, $q_{\rm dep,pk}$ is actually reduced with sufficient lithium evaporation, in this case 300 mg is used, from 5.5 MW m$^{-2}$ to 2.5 MW m$^{-2}$. The result is a clear reduction in the power deposited by the plasma at the outer strike point. When only 150 mg of lithium evaporation is employed, the divertor heat flux at the outer strike point is similar to the boronized reference discharge. This indicates that there is a threshold amount of lithium influx into the divertor required to achieve a reduction in the deposited heat flux.

### 3.1. Heat flux

The effects of increasing lithium deposition on power accounting at the outer strike point in divertor can be seen in figure 4, where $P_{\rm div}^{\rm IR}$ is the divertor power and is determined by integrating the measured divertor heat flux from IR thermography and assuming axisymmetry. Divertor power accounting is then defined at the ratio of $P_{\rm div}^{\rm IR}/P_{\rm SOL}$. A ratio of $P_{\rm div}^{\rm IR}/P_{\rm SOL} = 1$ would indicate that all of the power crossing the LCFS is reaching the divertor. For 0 mg (boronized) discharges, $P_{\rm div}^{\rm IR}/P_{\rm SOL}$ ranges from 0.35–0.5. With the addition of 150 mg of lithium, divertor power accounting improves to $0.75 \leqslant P_{\rm div}^{\rm IR}/P_{\rm SOL} \leqslant 1$. However, increasing the lithium deposition to 300 mg reduces $P_{\rm div}^{\rm IR}/P_{\rm SOL}$ to between 0.125–0.2. Figure 5 shows time traces of $I_{\rm p}$ and the measured divertor surface temperature at the outer strike point, $T_{\rm surf,OSP}$ and $q_{\rm dep,pk}$ over the entire discharges shown in figure 2. A clear reduction in $T_{\rm surf,OSP}$ is observed in figure 5(*b*) for these 0.8 MA shots that are otherwise nearly identical. There are differences in the gas puff rate used to fuel each discharge since a significant increase in fuelling is required for the 300 mg discharge. Similarly, due to the increased lithium evaporation, ELMs are mitigated and the impurity content in the core plasma is higher. Therefore, $P_{\rm rad}^{\rm core}$ is increased for the 300 mg discharge. However, from figure 2(*c*), the difference in $P_{\rm SOL}$ is only significant during the initial NBI pre-heating from 0.1–0.25 s.

$T_{\rm surf,OSP}$ is reduced by 40–50% with increased pre-discharge lithium evaporation, which leads to a reduction in the computed heat flux. Figure 5(*c*) shows a reduction from $q_{\rm dep,pk} = 5$ MW m$^{-2}$ to $\leqslant 3$ MW m$^{-2}$ at $t = 0.4$ s. $q_{\rm dep,pk}$ tends to decrease as the discharge progresses due to a secular density rise in the core plasma [3]. Because of this, comparison of the 2 discharges is typically limited to discharges times after the H-mode transition is achieved and but prior to $q_{\rm dep,pk}$ beginning to roll-over due to the secular density rise. $q_{\rm dep,pk}$ for the 150 mg discharge only approaches $q_{\rm dep,pk}$ for the 300 mg discharge around $t = 0.8$ s. While only two discharges are being compared in figure 5, the trend remains intact for all $I_{\rm p}$ and $P_{\rm NBI}$ conditions observed to date in NSTX. This can be seen in figure 6 where the 150 mg data shows $q_{||,\rm pk}$ linearly increasing with increasing $I_{\rm p}$. The 300 mg data shows a similar linear trend with some overlap with the 150 mg dataset except $q_{||,\rm pk}$ is in general lower compared to the 150 mg data. The 300 mg data also appears to flatten for $I_{\rm p} \geqslant 1.1$ MA though

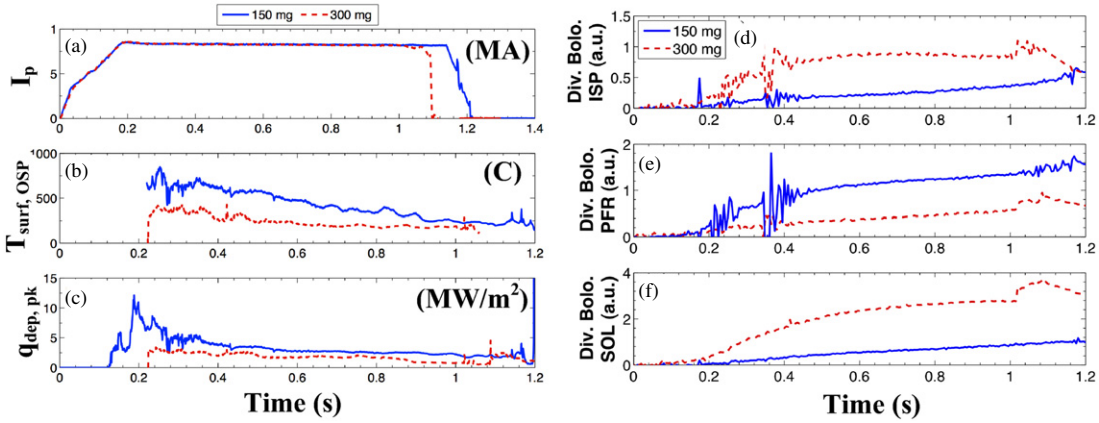


**Figure 5.** (*a*) $I_p$ (shown again for reference); (*b*) divertor surface temperature at the outer strike point, $T_{surf,OSP}$; (*c*) peak deposited heat flux, $q_{dep,pk}$ and relative changes in divertor radiation measurements from three bolometry chords located at (*d*) the inner strike point (ISP), (*e*) the private flux region (PFR), (*f*) the far scrape-off layer (SOL) for the lithium discharges shown previously in figure 1(*b*).

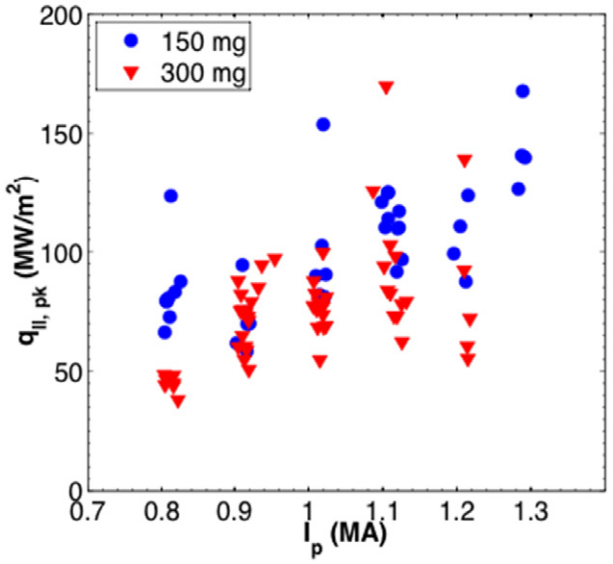


**Figure 6.** Peak parallel divertor heat flux, measured at the outer strike point versus $I_p$ for 150 and 300 mg of pre-discharge lithium evaporation for $P_{NBI} = 4$ MW and $\delta \sim 0.7$.

more data at higher $I_p$ will be required to determine if the trend continues.

Figures 5(*d*)–(*f*) show the relative changes in divertor radiation as measured by divertor bolometry. The divertor bolometer sight lines, shown in figure 1(*b*), look through the core plasma. From figure 2(*f*), the magnitude of the core radiation for the two discharges is similar up to 0.6 s and does not diverge significantly until 0.8 s. Therefore, comparison of the divertor bolometry data from the 150 and 300 mg discharges is still possible since the contribution from the core plasma is similar between the two discharges at times early in the discharges. Figure 5(*d*) shows that divertor radiation at the inner strike point (ISP) is a factor of 4 higher in the 300 mg discharge than the 150 mg discharge early in the discharge ($t \leqslant 0.6$ s). Figure 5(*f*) shows similar trends at the OSP. Conversely, figure 5(*e*) shows the opposite trend in the private flux region (PFR). Divertor radiation is increased for the lower lithium deposition amounts by also the same factor of 4. The reason for this is still under investigation, but could be due to the reduction in MARFE activity in the X-point region with lithium as has been shown previously in discharges that utilize lithium wall condition [22]. However, the lack of more extensive divertor bolometric coverage prevents a confirmation of this hypothesis.

**Table 1.** Divertor $T_e$ and $n_e$ determined from a divertor Langmuir probe located at $r = 0.495$ m in the far SOL at $t = 0.4 \pm 0.050$ s for the 150 and 300 mg discharges shown in figure 5.

| | $j_{sat}$ (kA m$^{-2}$) | $T_e$ (eV) | $n_e$ (m$^{-3}$) |
|---|---|---|---|
| 150 mg (141255) | $3.5 \times 10^3$ | 21 | $4.3 \times 10^{19}$ |
| 300 mg (138240) | $3.9 \times 10^3$ | 15 | $7.4 \times 10^{19}$ |

Langmuir probe measurements are available from one probe located at $r = 0.495$ m. The probe data are averaged from $t = 0.4 \pm 0.050$ s. During this time, the probe is located in the near SOL of the 150 mg and 300 mg discharges ($\psi_N = 1.04$ and 1.06, respectively). From these measurements, shown in table 1, there is an increase in divertor electron density from $4.3 \times 10^{19}$ to $7.4 \times 10^{19}$ m$^{-3}$ an increase of 70%, while the electron temperature drops from 21 to 15 eV with the increased lithium evaporation. Further, if the heat flux to the probe is estimated as, $q_{probe} \propto j_{sat} T_e^{3/2}$ and the sheath heat transmission factors are similar between the 150 and 300 mg discharges, than the relative decrease in the probe heat flux is similar to the decrease in heat flux measured by the dual-band IR system.

### 3.2. SOL width

Previous work has reported on the scaling of the power exhaust width, $\lambda_q$ on NSTX with $I_p$ and $P_{SOL}$ for boronized wall conditions [3, 23]. There it was found that the integral definition [24] of $\lambda_q$ magnetically mapped to the midplane, $\lambda_{q,int}^{mid}$, where $\lambda_{q,int}^{mid} = \lambda_{q,int}^{div}/f_{exp}$, scales proportional to $I_p^{-1.6}$ for boronized, attached divertor conditions. Here we also use the semi-empirical definition for $\lambda_q$ that assumes that the radial heat flux profile can be described by a diffusive-Gaussian equation [25] given by:

$$q(\bar{s}) = \frac{1}{2} q_0 \exp\left(\left(\frac{S}{2\lambda_q f_{exp}}\right)^2 - \frac{\bar{s}}{\lambda_q f_{exp}}\right) \times \mathrm{erfc}\left(\frac{S}{2\lambda_q f_{exp}} - \frac{\bar{s}}{S}\right) + q_{BG}, \quad (1)$$

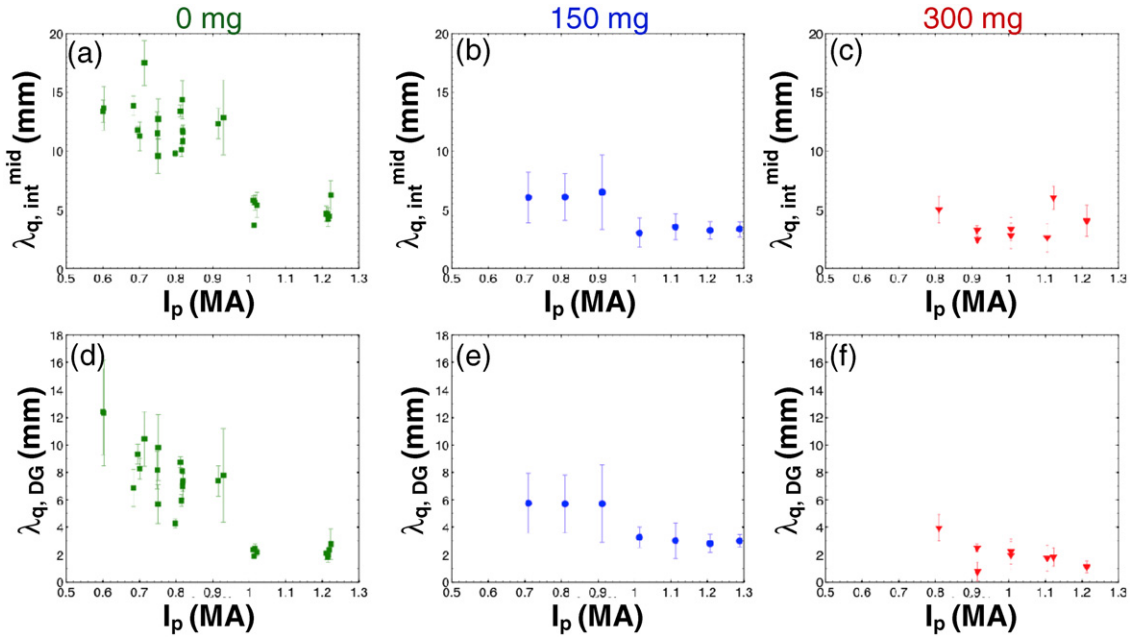


**Figure 7.** Inter-ELM averaged (30 Hz) $\lambda_{q,\mathrm{int}}^{\mathrm{mid}}$ and $\lambda_{q,\mathrm{DG}}$ as a function of $I_\mathrm{p}$ for 0 mg (∗), 150 mg (●) and 300 mg (▼) pre-discharge lithium evaporations where $\delta \sim 0.7$ and $P_\mathrm{NBI} = 4$ MW.

where $s$ is the radial coordinate, $s_0$ the strike point location, $\bar{s} = s - s_0$, $q_0$ is the peak heat flux, $q_\mathrm{BG}$ is the background heat flux, $\lambda_q$ is the $e$-folding length of the heat flux profile at the midplane and $S$ is the diffusive parameter and represents heat that has diffused into the PFR. For clarity, this $\lambda_q$ is referred to as $\lambda_{q,\mathrm{DG}}$ to distinguish it from $\lambda_{q,\mathrm{int}}$. Figure 7 shows how the inter-ELM measurements of $\lambda_{q,\mathrm{DG}}$ and $\lambda_{q,\mathrm{int}}^{\mathrm{mid}}$ vary as a function of $I_\mathrm{p}$ and lithium deposition. The measurements in figure 7 are shot averaged to provide better statistics and error in the measurements is derived from the standard deviation measurements for a single discharge. Regardless of the lithium deposition, $\lambda_{q,\mathrm{int}}^{\mathrm{mid}}$ and $\lambda_{q,\mathrm{DG}}$ both follow similar power law scalings $\propto I_\mathrm{p}^{-\alpha}$ with $\alpha$ decreasing with increasing lithium deposition. However, at high $I_\mathrm{p}$, $\lambda_{q,\mathrm{DG}} \sim 2$ mm regardless of the amount of pre-discharge lithium evaporation.

The diffusive parameter, $S$ is also found to contract with $I_\mathrm{p}$. From figure 4 it was shown that divertor power accounting, as measured by the ratio of $P_\mathrm{div}^\mathrm{IR}/P_\mathrm{SOL}$, changes dramatically with lithium deposition. Figure 8 shows how $S$ varies as a function of $1 - (P_\mathrm{div}^\mathrm{IR}/P_\mathrm{SOL})$. From this it is apparent that while $S$ for discharges with 150 mg of lithium is slightly greater on average than 0 mg discharges, there is significant scatter in both data and $S$ is approximately constant between 10 and 15 mm for these discharges. Conversely, $S$ for 300 mg discharges range from 14 to 29 mm as $1-(P_\mathrm{div}^\mathrm{IR}/P_\mathrm{SOL})$ increases from 0.7–0.9. Therefore, there is a good correlation between increased heat flux diffusion into the PFR as divertor power accounting decreases.

### 3.3. Progressively increased lithium deposition

Heat flux data, taken during the 2008 run campaign and discussed in the literature [15–17], show trends in $\lambda_{q,\mathrm{DG}}$ and $S$ as pre-discharge lithium evaporation is progressively increased. These discharges are lower $\delta$ (∼0.5) with

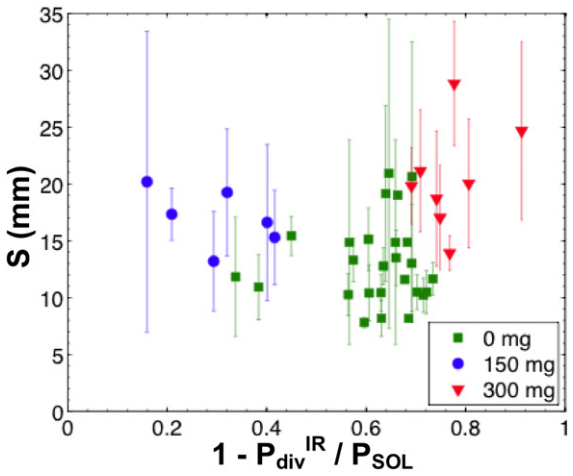


**Figure 8.** Variations in the diffusive parameter $S$ versus $1 - (P_\mathrm{div}^\mathrm{IR}/P_\mathrm{SOL})$ for 0 mg (∗), 150 mg (●) and 300 mg (▼) pre-discharge lithium evaporation.

$P_\mathrm{NBI} = 2$–4 MW. Lower beam power was required as the lithium deposition was increased due to global stability limits being reached that lead to disruptions. This data also predates the dual-band IR camera system on NSTX and as such the magnitude of the heat flux is questionable, but previous observations [3] show that the overall shape of the heat flux profile is consistent between single and dual-band IR measurements. The heat flux data for $t = 0.25$–0.45 were non-linearly fit to equation (1) for each discharge and then averaged over a time window of 0.25–0.45 s which was chosen to ensure data were during the H-mode but prior to the density roll-over typically seen in NSTX heat flux data [3]. Figure 9(*a*) shows that $\lambda_{q,\mathrm{DG}}$ decreases with the addition of more pre-discharge lithium evaporation. Since these data are inter-ELM averaged at 30 Hz, some of this decrease is due to suppression of small type V ELMs which can be ubiquitous in NSTX discharges.

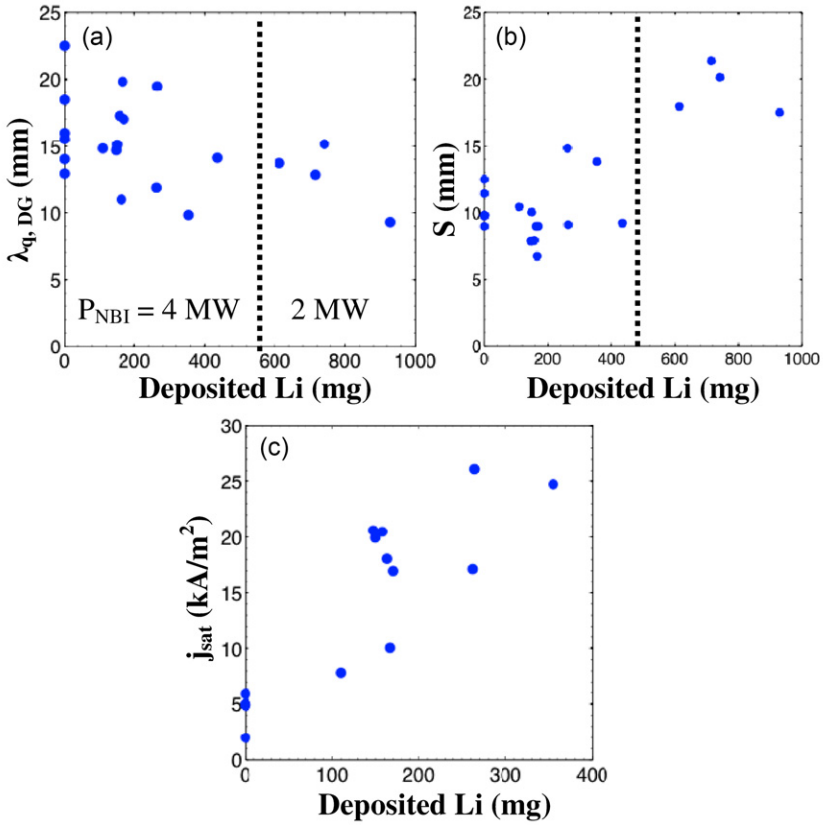


**Figure 9.** Inter-ELM averaged (30 Hz) (*a*) $\lambda_{q,\mathrm{DG}}$, and (*b*) $S$ for $P_{\mathrm{NBI}} = 2$–4 MW and (*c*) $j_{\mathrm{sat}}$ from a divertor Langmuir probe located at $r = 0.91$ m as a function increasing lithium deposition.

However, the decrease in $\lambda_{q,\mathrm{DG}}$ continues after ELMs have been fully suppressed. The continued decrease in $\lambda_{q,\mathrm{DG}}$ could be due to continued pedestal modification [24] by increasing lithium deposition.

The diffusive parameter $S$, as seen in figure 9(*b*), is unaffected or decreases slightly between 0 and 200 mg of lithium and then increases with further increases in lithium deposition. The increase in lithium deposition appears to be correlated with increased diffusion of the heat flux into the PFR. This appears to be due to the increase in divertor particle flux, as measured by a divertor Langmuir probe located in the SOL, that results with increased lithium deposition as shown in figure 9(*c*). The data in figure 9(*c*) has been limited to <400 mg of lithium because of the necessary reduction in $P_{\mathrm{NBI}}$ to 2 MW to avoid global MHD modes.

## 4. Conclusions

Here we present heat flux data obtained on NSTX with varying amounts of pre-discharge lithium evaporation. Heat flux was determined by measuring the surface temperature of the divertor with a dual-band IR camera to reduce the effect of variable surface emissivity introduced by the lithium coatings. These measurements show not only a contraction in the heat flux footprint, but also a reduction in the magnitude of the peak heat flux when a threshold amount of lithium is used. The reduction in heat flux, even with a significantly contracted $\lambda_q$, shows an increase in divertor power accounting, as measured by the ratio of $P_{\mathrm{div}}^{\mathrm{IR}}/P_{\mathrm{SOL}}$, with 150 mg when compared to boronized (0 mg) discharges. However, when the lithium deposition is increased to 300 mg, power accounting drops to between 12.5 and 20% of $P_{\mathrm{SOL}}$. The decrease in divertor heat flux is accompanied by a relative increase in radiation at the inner strike point as well as in the far SOL of the divertor when comparing the 300 mg to the 150 mg discharge. However, radiation measured from the PFR is reduced with higher lithium deposition amounts. The reason for this is not well understood and modelling is planned to help address this issue. The contraction in the heat flux footprint, $\lambda_{q,\mathrm{DG}}$ appears to be proportional to both $I_{\mathrm{p}}$ and the amount of lithium deposited with the differences in $\lambda_{q,\mathrm{DG}}$ largely undistinguishable at high $I_{\mathrm{p}}$ where $\lambda_{q,\mathrm{DG}} \sim 2$–4 mm regardless of the amount of lithium deposition. Additionally, the diffusive parameter $S$ increases with lithium deposition above 200 mg but decreases between 0 and 200 mg of lithium. The initial decrease in $S$ is believed to be due to reduced divertor recycling from the lithium; while the increase in $S$ above 200 mg is correlated to increased particle flux in the SOL. The increased divertor flux increases the divertor collisionality and leads to increased diffusion of heat flux into the PFR and increased divertor radiation. The use of lithium to moderate divertor heat fluxes requires a threshold amount of lithium to achieve this. For high $\delta$, high performance NSTX discharges, lithium deposition >200 mg appears to be the threshold required for reduction in the peak heat flux to the divertor.

## Acknowledgments

Work supported by US Department of Energy contracts: DE-AC05-00OR22725, DE-AC52-07NA27344 and

DE-AC02-09CH11466. The authors would also like to acknowledge a collaboration with A Herrmann of IPP-Garching for the use of the THEODOR code. The authors would also like to acknowledge useful discussions with T Eich regarding the diffusive-Gaussian heat flux analysis.

## References

[1] Loarte A. *et al* 2007 *Nucl. Fusion* **47** S203
[2] Menard J.E. *et al* 2010 *Proc. 37th EPS Conf. Plasma Physics (Dublin, Ireland, 2010)* http://ocs.ciemat.es/EPS2010PAP/P2.106.pdf
[3] Gray T.K. *et al* 2011 *J. Nucl. Mater.* **415** S360–4
[4] Soukhanovskii V.A. *et al* 2009 *Nucl. Fusion* **49** 095025
[5] Soukhanovskii V.A. *et al* 2009 *Phys. Plasmas* **16** 022501
[6] Ryutov D.D. 2007 *Phys. Plasmas* **14** 064502
[7] Soukhanovskii V.A. *et al* 2011 *J. Nucl. Mater.* **415** S365–8
[8] Jaworski M.A. *et al* 2013 *Nucl. Fusion* **53** 113030
[9] Mazzitelli G. *et al* 2011 *Nucl. Fusion* **51** 073006
[10] Mirnov S. 2009 *J. Nucl. Mater.* **390–391** 876885
[11] Sanchez J. *et al* 2011 *Nucl. Fusion* **51** 094022
[12] Bell M.G. *et al* 2009 *Plasma Phys. Control. Fusion* **51** 124054
[13] Kaye S.M. *et al* 2011 *Nucl. Fusion* **51** 113019
[14] Guo H.Y. *et al* 2011 *J. Nucl. Mater.* **S415** S369–74
[15] Maingi R. *et al* 2011 *Phys. Rev. Lett.* **105** 145004
[16] Maingi R. *et al* 2009 *Phys. Rev. Lett.* **103** 075001
[17] Kugel H.W. *et al* 2008 *Phys. Plasmas* **15** 056118
[18] Mastrovito D.M. *et al* 2003 *Rev. Sci. Instrum.* **74** 5090–2
[19] Ahn J.-W. *et al* 2010 *Rev. Sci. Instrum.* **81** 023501
[20] McLean A.G. *et al* 2012 *Rev. Sci. Instrum.* **83** 053706
[21] Herrmann A. 2001 *Proc. 28th EPS Conf. Controlled Fusion and Plasma Physics (Madeira, Portugal, 2001)* www.cfn.ist.utl.pt/EPS2001/fin/authors/nav/AutH02fr.html
[22] Scotti F. *et al* 2011 *J. Nucl. Mater.* **S415** S405–8
[23] Maingi R. *et al* 2007 *J. Nucl. Mater.* **363–365** 196–200
[24] Loarte A. *et al* 1999 *J. Nucl. Mater.* **266–269** 587–92
[25] Eich T. *et al* 2011 *Phys. Rev. Lett.* **107** 215001
[26] Boyle D. *et al* 2013 *J. Nucl. Mater.* **438** S979–82